

Equivalent Circuit Analysis Of The SLAC Damped Detuned Structure^{*}

R.M Jones^{†‡}, K. Ko[†], N.M. Kroll^{†‡}, R.H. Miller[†] & K.A. Thompson[†]

[†]Stanford Linear Accelerator Center, M/S 26, P.O Box 4349, Stanford, CA 94309

[‡]University of California, San Diego, La Jolla, CA 92093-0319.

1. ABSTRACT AND INTRODUCTION

The Damped Detuned Structures (DDS) currently under construction to serve as accelerating cavities for the NLC Test Accelerator (NLCTA) incorporate both damping and detuning as a means of suppressing the transverse wakefield. Detuning is accomplished by systematic variation of cell parameters so as to produce a spread in the frequencies of the dipole modes excited by the beam, and damping is accomplished by coupling the individual cells to four waveguide-like structures (called damping manifolds) that run parallel to the cavity and propagate dipole mode energy to loads coupled to the ends of these manifolds. The details of the DDS as well as the rationale underlying its design are discussed in [1]. It differs from previously considered designs [2] in that the manifolds have only one propagating mode in the frequency range of interest and also in that, like the cells, their parameters vary along the structure. The previously reported equivalent circuit analysis [2] has been elaborated in the following respects: (1) The treatment of the manifolds has been modified so as to take account of the effect of its coupling to the cells on its propagation characteristics and also to include the effect of their cell-to-cell variation. (2) The manifold-to-cell coupling network has been modified to take account of the TE₁₀ like character of the manifold propagating mode. (3) The chain of resonant circuits intended to represent the cells has been doubled (following Bane-Gluckstern [3]) to take account of the mixed TE-TM character of the dipole modes.

2. EQUIVALENT CIRCUIT ANALYSIS

The equivalent circuit which we use to represent the structure is shown in Fig. 1. The LC circuits represent the TE and TM components of the dipole field of the individual cells. Each component is magnetically coupled to both components of the adjacent cells. The electron beam excitation of the cavity is modeled by the input currents to each of the TM cells. The manifold structure is modeled by the uppermost sequence of transmission line sections each carrying a TE₁₀ waveguide mode and shunted by an LC circuit at the junction of adjacent transmission lines. Coupling of the accelerator cells to the manifolds is represented by a coupling between the

shunt capacitance of the manifold and the capacitance of the TE component of the corresponding accelerator cell:

$$V_n = -j(I_n / C_n + i_n \kappa_n / \sqrt{C_n c_n}) / \omega \quad (1)$$

$$v_n = -j(i_n / c_n + I_n \kappa_n / \sqrt{C_n c_n}) / \omega$$

where (C_n, c_n) represent the manifold shut capacitance and TE cell capacitance respectively, (V_n, v_n) the corresponding voltages across them, and (I_n, i_n) the currents through them. Thus the dimensionless quantity κ_n provides the manifold-cell coupling.

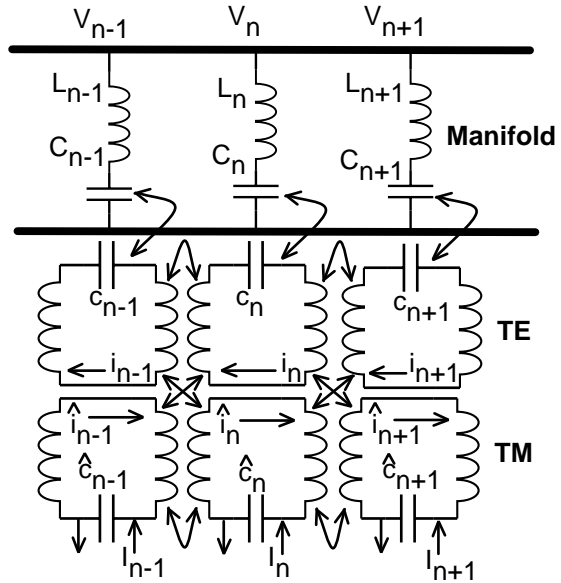


Figure 1: Circuit Model of DDS

The network equations for the circuit in Fig. 1 can be written in the form given below (the detailed relations between the circuit parameters are given elsewhere [4]).

$$RA = Ga \quad (a)$$

$$(H - 1/f^2)a + H_x \hat{a} = GA = GR^{-1}G \quad (b) \quad (2)$$

$$(\hat{H} - 1/f^2)\hat{a} + H_x^t a = B/f^2 \quad (c)$$

Here a , \hat{a} , and A are N ($N=206$) component vectors proportional to the loop currents (i_n) in the TE circuits, the loop currents (\hat{i}_n) in the TM circuits, and the shunt voltages (V_n) , in the manifolds respectively. B is also an N component vector proportional to the driving currents. R , H , \hat{H} , H_x and its transpose H_x^t , and G are $(N \times N)$

^{*} Supported by DOE grant number DE-FG03-93ER40759[†] and DE-AC03-76SF00515[†]

matrices. Their non-zero matrix elements have the following form:

$$R_{nn} = -2\cos\phi_n, \quad R_{n\pm 1} = 1 \quad (3)$$

$$\cos\phi_n = \cos\phi_{0n} - \alpha_n (\pi L f / c)^2 F_n^2 / (F_n^2 - f^2) \text{sinc}\phi_{0n} \quad (4)$$

$$\phi_{0n} = (2\pi L / c) \sqrt{f^2 - F_{cn}^2} \quad (5)$$

$$H_{nn} = 1 / f_n^2 + \Gamma_n^2 / \alpha_n / (F_n^2 - f^2) \quad (6)$$

$$H_{n\pm 1} = \eta_{n\pm 1/2} / (2f_n \hat{f}_{n\pm 1}) \quad (7)$$

$$H_{x,n\pm 1} = \pm \eta_{x,n\pm 1/2} / (2f_n \hat{f}_{n\pm 1}) \quad (7)$$

$$\hat{H}_{nn} = 1 / \hat{f}_n^2, \quad \hat{H}_{n\pm 1} = -\hat{\eta}_{n\pm 1/2} / (2\hat{f}_n \hat{f}_{n\pm 1}) \quad (8)$$

$$G_{nn} = \Gamma_n (\pi L / c) F_n^2 / (F_n^2 - f^2) \sqrt{\text{sinc}\phi_{0n}} \quad (9)$$

There are nine n -dependent parameters per cell exhibited in the above equations. We discuss them below. The quantity ϕ_n represents the local phase advance per section of the manifold regarded as a quasi-periodic structure with slowly varying properties. Three parameters are required for its description: F_c corresponding to the cutoff of the local waveguide section, F to the resonant frequency of the series capacitance-inductance shunt, and α to the shunt capacitance itself. The n -independent parameter L is the section length, and for our structure is equal to one third the wavelength of the accelerating field. In writing eqs. (3) and (4) we have omitted terms second order in the section-to-section variation. The quantities f_n , \hat{f}_n correspond to the resonant frequencies of the TE and TM component of the cells, respectively, when the Γ 's and η 's are neglected. The three η 's represent the mutual inductances of Fig. (1) in an obvious way. The ninth parameter, Γ , represents the manifold-to-TE coupling. It is a function of α and κ and is used in place of κ .

With Γ_n set equal to zero, the cell equations become identical to those of [3], and the explicit connection of the relevant parameters to the circuit can be found there. The source vector B in eq. (2c) is expressed in terms of cell kick factors in precisely the same manner as in sections 2.3 and 3.2 of [3]. Also we follow [3] in terminating the chain of cells as implied by simply requiring, $n, n \pm 1$ to all belong to the set $\{1, \dots, N\}$. In this paper, we terminate the manifold with an outgoing wave boundary condition, which can be shown to require that we replace R_{11} and R_{NN} by $-\exp(j\phi_1)$ and $-\exp(j\phi_N)$ respectively. For most purposes we eliminate the explicit appearance of the manifold amplitude vector A by using eq. (2a) to bring the RHS of eq. (2b) to the second form shown.

3. THE DETERMINATION OF THE PARAMETERS

The parameters are determined by fitting to the frequency versus phase advance dispersion curves of the three lowest modes of strictly periodic structures having the dimensions of a selected representative set of cell dimensions. These are determined from MAFIA frequency domain simulations of a single section with specified phase advance boundary conditions. The

dispersion relation is obtained from eqs. (2) using the definitions in eqs. (3) to (9) and is as follows:

$$\begin{aligned} & \left\{ \left[(1 + \eta \cos \psi) / f_0^2 + \Gamma^2 / \alpha / (F^2 - f^2) - f^{-2} \right] \right. \\ & \left. \left[(1 - \hat{\eta} \cos \psi) / \hat{f}_0^2 - f^{-2} \right] - \eta_x^2 / (f_0 \hat{f}_0) \sin^2 \psi \right\} \\ & [\cos \psi - \cos \phi] = \\ & \Gamma^2 F^2 / (F^2 - f^2) (\pi L / c)^2 \left[(1 - \hat{\eta} \cos \psi) \hat{f}_0^{-2} - f^{-2} \right] \text{sinc} \phi \end{aligned} \quad (10)$$

As an example of the procedure, we illustrate its application to cell 106 in Fig. (2).

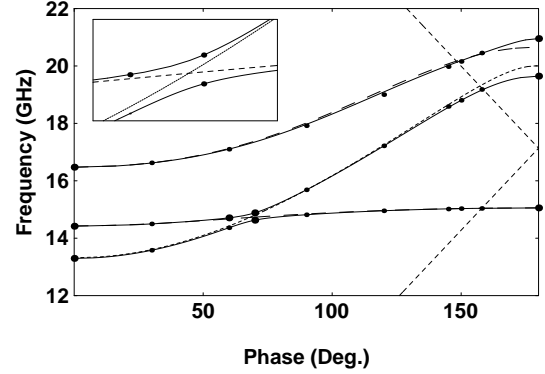


Figure 2: Brillouin Diagram for Cell 106 (Avoided Crossing shown inset)

The parameters are determined by requiring that the three curves pass through nine selected phase-frequency pairs (the large dots in Fig. (2)) determined from simulations. The 0 and π phase advance points provide six pairs, and three points near the avoided crossing provide the rest. The dashed curves are obtained by setting the RHS of eq. (10) to 0. They represent the dispersion curves of the lower and upper dipole modes and of the manifold mode when direct manifold-cell coupling is suppressed. The smaller dots in Fig. (2), also from simulations, are used to assess the quality of the fit rather than for parameter determination. As discussed in [2], effective damping is associated with the crossing of the lower dipole mode and the manifold mode. When the coupling is included the crossing is avoided as shown by the solid curves. The cell kick-factors required both to relate the current source to a driving bunch and to compute the transverse kick which it imparts to a trailing bunch [3] are also determined from the simulations.

The parameter determination is carried out as above for eleven selected cells. A smooth fit as a function of cell number is then formed to provide values for all of the cells and also for quantities with half integer designations.

4. DETERMINATION OF THE WAKE FUNCTION

We have evaluated the wake function function (rather loosely referred to as a wakefield in [1,2 &3]) by means of the modal expansion method, both perturbative as discussed in [2] and non-perturbative as discussed in [1] (see eq. (2)). The unperturbed mode distribution function

and the kick-factor weighted mode distribution function, both obtained by setting G equal to zero in eq. (2b), are shown in Fig. (3 inset) and Fig. (3) respectively. They should be compared to Fig. (19) a and c of [3]. Because of the f dependence in H_m , the computational problem of obtaining the modes is somewhat more involved than for the corresponding problem in [3], but a straightforward iteration procedure proved to be rapidly convergent.

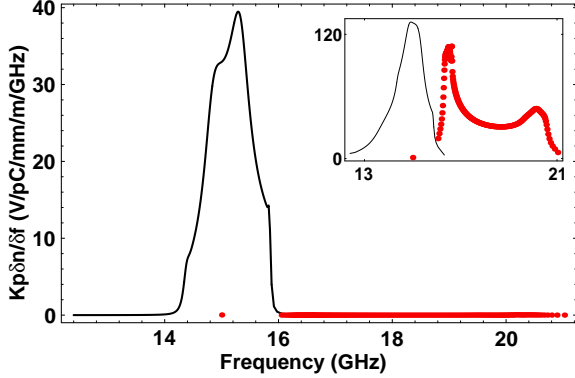


Figure 3: Kick-Factor Weighted Density Function (Density Function, $\delta n/\delta f$, shown inset)

It also leads to a slight change in the expression for the modal kick-factors. Over the synchronous frequency band of the lower dipole mode the perturbative Q varies from 753 to 1089 with a mean value of 956. The upper dipole mode is not significantly damped by the manifolds because they are non-propagating over most of the band and lack avoided crossings where they are propagating. In contrast to our previous experience [1], the non-perturbative method proved to be numerically quite challenging and excessively time consuming. As pointed out previously [1,2], the complication arises from the fact that the matrix is complex symmetric rather than real symmetric, with all elements dependent upon frequency in a complicated way. An iterative method based upon repeated determination of eigenvalues was used rather than the determinantal method described in [1].

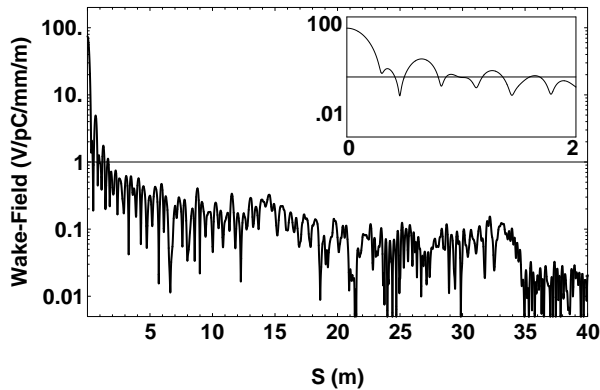


Figure 4: Envelope of Wake Function

Both the real and imaginary parts of the frequency shift showed large rather regular oscillations about the

perturbative values, large changes in the kick-factors, and large phase shifts in the modal sinusoids [1]. (These phase shifts represent the phase of the complex modal kick factors whose absolute value is given by K_p [4]). The resultant wake function, shown in Fig. (4) and including the upper band contribution, is significantly but not drastically degraded from the perturbative form (not shown). On the other hand, the short range behavior (inset) is hardly changed. This is just what one expects on physical grounds, but the fact that it emerges from very different input data encourages us to trust our results. As discussed in [5] the short range behavior is determined by $K_p \delta n/\delta f$ in Fig. (3), and the differences between it and Fig (19c) of [3] accounts for the poorer short distance damping achieved by this version of the DDS design.

5. DISCUSSION

While we believe that the short range behavior of the wake function shown in Fig. 5 can be improved by a redesign, the overall behavior is considered to be quite satisfactory. There are, however, a number of departures in the actual structure from the design analyzed here. The termination of the structure on each end will involve modification of the last few cells and also a loading structure. Our method is flexible enough to take these changes into account once the appropriate input data has been obtained. The fact that the current design is too strongly coupled to allow us to rely upon perturbation theory has been a handicap, however. In order to ameliorate this problem we have developed a new method involving integration along real branch cuts rather than the modal expansion. It has turned out to be much more efficient numerically and is also closer to an exact treatment. Its comparison with the method reported here and its application to the structure including the modifications mentioned above will be reported in [4,5].

6. ACKNOWLEDGMENTS

The authors R.M.J. and N.M.K. are very grateful for the insight provided in discussions with K.L.F. Bane. We have also benefited greatly from discussions at the weekly structures meeting at SLAC, where these results were first presented and thank all members of the group.

7. REFERENCES

- [1] K.Ko, et al, 16th IEEE Particle Accelerator Conference, Dallas, TX, 1995, SLAC-PUB-6844
- [2] N.M. Kroll et al, AIP Conf. Proc., **335**, 777-788 (AIP Press,1995), SLAC-PUB-6660
- [3] K.L.F. Bane & R.L. Gluckstern, Part. Accel., **42**, 123 1993; SLAC-PUB-5783
- [4] R.M. Jones, et al, paper in preparation.
- [5] R.M. Jones, et al, 18th Intl. Linac Conf., Geneva, Switzerland,1996